REVISTA COLOMBIANA DE COMPUTACIÓN
Volumen 11, número 2
Págs. 79 - 93

Carotid arteries segmentation in CT images with use of a right generalized cylinder model

Leonardo Flórez Valencia* Jacques Azencot
Maciej Orkisz†

Fecha de Recibido: 24/05/2010 Fecha de Aprobación: 25/10/2010

Abstract

The arterial lumen is modeled by a continuous right generalized cylinder with piece-wise constant parameters. The method is based on the identification of the parameters of each piece from a series of contours extracted along an approximate axis of the artery. This curve is defined by a minimal path between the artery end-points. The contours are extracted using the Fast Marching algorithm. The identification of the axial parameters is based on a geometrical analogy with helical curves, while the identification of the surface parameters uses the Fourier series decomposition of the contours. Thus identified parameters are used as observations in a Kalman optimal estimation scheme that manages the spatial consistency from each piece to another. The method was evaluated on 46 datasets from the MICCAI 3D Segmentation in the Clinic Grand Challenge: Carotid Bifurcation Lumen Segmentation and Stenosis Grading (http://cls2009.bigr.nl).

*Pontificia Universidad Javeriana, Departamento de Ingeniería de Sistemas, Bogotá, Colombia, florez-l@javeriana.edu.co.

† Université de Lyon; Université Lyon 1; INSA-Lyon; CNRS UMR5220; INSERM U630; CREATIS, F-69621 Villeurbanne, France, azencot@creatis.insa-lyon.fr, orkisz@creatis.insa-lyon.fr.

1 Introduction

Image segmentation plays an increasing role in today's assessment of vascular diseases. Measurements inferred from the segmentation help the physician to evaluate the disease severity. For example, one important measure is the *stenosis degree*, indicating the percentage of lumen reduction of a pathological section compared to the healthy part of the vessel. Various approaches of vascular segmentation published over the past years are mainly based on *vessel tracking* and *deformable models* (see [6] for a review). *Vessel tracking* methods scan the vessel incrementally and progressively build a *discrete* (geometrical) *representation* of the vessel, usually composed by a centerline and a stacking of planar contours. It is important to note that this approach hardly exploits the 3D continuity of the vessel surface. On the other hand, *deformable models* are usually *discrete surfaces* (meshes) that deform their geometry to fit the data. The deformation is obtained by minimizing an objective function with two competitive terms: a *local constraint* (data attachment) and a *global constraint* (*a priori* on the geometrical shape). This approach does not provide direct access to clinically useful cross-sectional measures.

This work is motivated by applications involving the segmentation and the quantification of tubular-shaped objects, e.g. blood vessels, in medical three-dimensional (3D) images. Although healthy blood-vessels have cylindrical shapes with circular cross-sections, pathologies such as atherosclerosis, may lead to quite complex deformations of the cross-sectional shape.

A generalized cylinder model capable of representing complex elongated objects, using a reduced number of parameters, was proposed in [1]. The model is composed of two parts: the first one describing the axial shape by means of orthonormal bases attached to the axis, and the second one describing the surface by means of contours in the planes orthogonal to the axis. This model was called RGC-sm, which stands for right generalized cylinder state model, since the authors used the system-state formalism. According to this formalism, both components (the local base and the cross-sectional contour) corresponding to any arc-length location, can be calculated knowing only one initial base and contour, as well as their dynamics (parameters describing their variation). The main characteristics of RGC-sm are:

1. Piece-wise constant dynamics - the actual generalized cylinder is subdivided into segments such that all the state variables within a segment are constants, and

2. continuity - while continuously varying the arc-length, one obtains a continuous axis and surface.

A similar model was recently used in [7].

In [3] we proposed an image-segmentation framework based on RGC-sm, which makes use of the Kalman state estimator to determine the optimal values of the state variables in the consecutive cylinder pieces. The key point in this algorithm is an appropriate computation of image-based observations. For each cylinder piece, these observations are to be inferred from two contours extracted in the planes bounding the piece. In this paper we assume that the contour-extraction problem is resolved. The focus is a geometry-based reasoning that leads to the retrieval of the observations to be used as input of the Kalman filter.

Thus, this paper is organized as follows: section 2 describes the RGC-sm model, section 3 describes our vessel segmentation algorithm based on RGC-sm and, finally, section 4 presents the results of evaluating the method on 15 training and 31 testing datasets from the MICCAI 3D Segmentation in the Clinic Grand Challenge: Carotid Bifurcation Lumen Segmentation and Stenosis Grading (http://cls2009.bigr.nl).

2 Right generalized cylinder model

The RGC-sm model is an association of a generating curve H and a stack of contours describing the surface S (see figure 1).

The model is piece-wise, *i.e.* it assumes that a generalized cylinder can be subdivided into pieces such that the model parameters be constant within each piece separately. Each piece H_i of the generating curve is defined by its length Δ_i, curvature K_i, torsion τ_i, and by the azimuthal rotation angle $_i$, of the local basis $\Gamma_i,(t)$ attached to H_i, with respect to the corresponding Frenet frame (see figure 2).

Each piece S_i of the surface is a continuous stack of contours $c_i(t,\omega)$ defined by a tuple $\{Z_i,\Delta_i,\}$, where $Z_i=\{Z_{i,I} \mid C; -q \le I \le +q\}$ represents the Fourier coefficients describing the first contour in the piece, and $\Lambda_i = \{\lambda_{i,I} \mid C; -q \le I \le +q\}$ is an ordered set of $2q+1$ coefficients linearly transforming the contour along H_i.

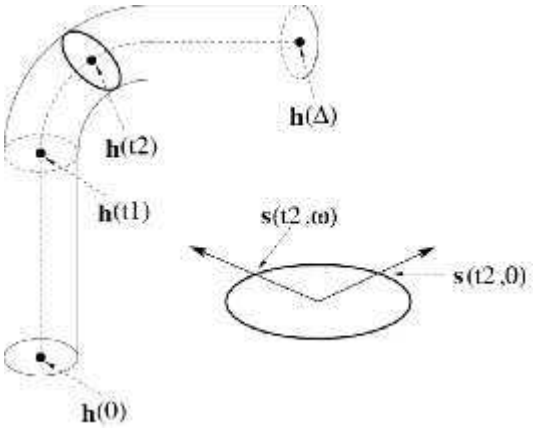

Fig. 1: Graphical representation of the RGC-sm parameters: the generating curve H_i (function $\boldsymbol{h}(t)$) and the surface S (function $\mathsf{s}(t,\omega)$). A representation (bottom-right) of the contour placed at $\boldsymbol{h}(t_2)$ is also shown.

Both coefficient sets are used to define contours as:

$$\mathbf{c}_i(t,\omega) = \sum_{l=-q}^{+q} (\lambda_{i,l}(t-t_i) + z_{i,l}) e^{jl\omega}, \qquad (1)$$

where t and ω respectively are arc-length and azimuthal parameters. The number q of harmonics controls the level of details of the contours, and thus of the whole generalized cylinder surface. Each surface piece S_i is connected to the corresponding generating curve piece H_i by the following equation:

$$\mathbf{s}_i(t,\omega) = \boldsymbol{\Gamma}_i(t) \begin{bmatrix} 0 \\ Re(\mathbf{c}_i(t,\omega)) \\ Im(\mathbf{c}_i(t,\omega)) \end{bmatrix} + \mathbf{h}_i(t), \qquad (2)$$

where $\boldsymbol{h}_i(t)$ is the spatial location of the origin of $\boldsymbol{\Gamma}_i(t)$, which belongs to $\mathbf{H}_i$. The entire model is thus:

$$\mathsf{M} \equiv \{\mathbf{h}_0, \boldsymbol{\Gamma}_0, \mathbf{Z}_0, \{\kappa_i, \tau_i, \nu_i, \Delta_i, \boldsymbol{\Lambda}_i; 0 \le i < n\}\}, \qquad (3)$$

where $\boldsymbol{h}_0 \equiv \boldsymbol{h}_0(t=0)$ is the first point of H, $\boldsymbol{\Gamma}_0 \equiv \boldsymbol{\Gamma}_0(t=0)$ is the first basis attached to $\boldsymbol{h}_0$ and $\boldsymbol{Z}_0 \equiv \boldsymbol{Z}_0(t=0)$ is the Fourier decomposition of the first RGC contour. An example of a RGC-sm is shown on figure 3.

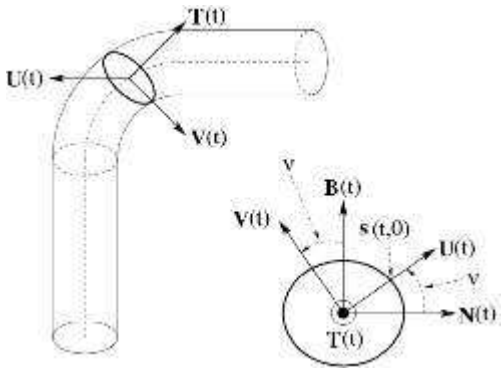

Fig. 2: Simple schema showing the connection between the base $\Gamma(t) = [\mathbf{T}(t)\ \mathbf{U}(t)\ \mathbf{V}(t)]$ and the Frenet frame $\mathbf{Fr}(t) = [\mathbf{T}(t)\ \mathbf{N}(t)\ \mathbf{B}(t)]$: the contour's first point is aligned with the vector $\mathbf{U}(t)$, which is the rotated version of $\mathbf{N}(t)$ around the vector $\mathbf{T}(t)$, by an angle .

Fig. 3: Example of a RGC-sm. Left: Surface representation. Right: Stack of contours. Note the presence of the generating axis.

3 Vessel tracking algorithm

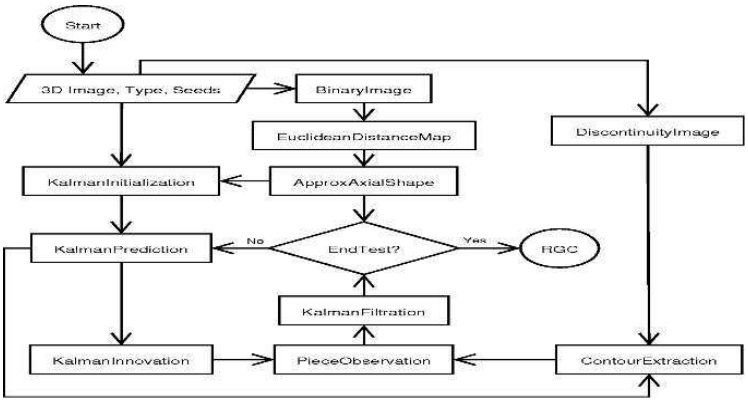

Fig. 4: Flowchart of the segmentation algorithm.

Figure 4 shows the global flowchart of the proposed algorithm for vascular segmentation. The vascular segment of interest is delimited by two points interactively given by the user. The *Kalman state estimator* (KSE) [8] (see section 3.1) is used to control the vessel tracking along an approximate axis between these points (see section 3.3). It predicts the 3D locations, orientations and shapes of the contours that delimit the consecutive cylinder pieces. The observation vector, coding the RGC-sm parameters of the i-th piece (see section 3.2), is computed from the result of the contour extraction performed in the predicted plane (see section 3.4). The observation is then filtered by the KSE to produce a corrected estimate of the parameters, which is expected to smooth out the possible errors of the contours and initial axis extraction. Only the very first contour remains uncorrected.

The KSE adapts the tracking speed to the complexity of the local vascular shapes (axial and superficial). In complex shapes (high local changes of curvature, for example) the length of the cylinder piece is automatically reduced. This occurs when the predicted contours are too different from the observations.

3.1 Kalman state estimator

The KSE, [8], addresses the general problem of estimation of the x-dimensional state $\mathbf{x} \in \mathbf{R}^x$ of a discrete-time controlled process that is governed by the linear stochastic difference equation:

$$\mathbf{x}_i = \mathbf{A}\ \mathbf{x}_{i-1} + \mathbf{B}\ \mathbf{u}_i + \mathbf{w}_{i-1} \qquad (4)$$

with a m- dimensional measurement $\mathbf{m} \in \mathbf{R}^m$:

$$\mathbf{m}_i = \mathbf{H}\ \mathbf{x}_i + \mathbf{v}_i \qquad (5)$$

where the random variables $\mathbf{w}_i$ and $\mathbf{v}_i$ represent, respectively, the process and measurement noises. These noises are assumed to be statistically independent between them, white and with normal probability distributions:

$$\begin{aligned} p(\mathbf{w}) &: N(0, \mathbf{Q}) \\ p(\mathbf{v}) &: N(0, \mathbf{R}) \end{aligned} \qquad (6)$$

where $\mathbf{Q}$ and $\mathbf{R}$ are the respective covariance matrices.

The xx x matrix $\mathbf{A}$ in equation 4 relates the state at the previous step i - 1 to the state at the current step i, in the absence of either a driving function or process noise. The x x u matrix $\mathbf{B}$ relates the optional u -

dimensional control input $\mathbf{u} \in R^u$ to the state $\mathbf{x}$. The mx x matrix $\mathbf{H}$ in the measurement equation 5 relates the state to the measurement $\mathbf{m}$.

The KSE algorithm is basically a loop that updates the ``time" i by projecting (predicting) the previous estimated state $\hat{\mathbf{X}}_{i-1}$ to $\hat{\mathbf{X}}_i^-$ and then correcting this prediction using the current measurement $\mathbf{m}_i$ to obtain the newly estimated (innovated) state $\hat{\mathbf{X}}$. Furthermore, a measure of the error estimation of the process is kept in the x x x matrices $\mathbf{P}_i$. The pseudo-code of the KSE is written in algorithm 1:

$\mathbf{Q}, \mathbf{R} \leftarrow InitNoises()$

$\hat{\mathbf{x}}_0 \leftarrow InitState()$

$\mathbf{P}_0 \leftarrow InitProcessNoise()$

while $\neg StopCriteria$:

$\mathbf{u}_i \leftarrow LoadInput(i)$; **Load current input**

$\hat{\mathbf{x}}_i^- = \mathbf{A} \cdot \hat{\mathbf{x}}_{i-1} + \mathbf{B} \cdot \mathbf{u}_i$; **Predict next state**

$\mathbf{P}_i^- = \mathbf{A} \cdot \mathbf{P}_{i-1} \cdot \mathbf{A}^T + \mathbf{Q}$; **Predict the process noise**

$\mathbf{K}_i = \mathbf{P}_i^- \cdot \mathbf{H}^T \cdot (\mathbf{H} \cdot \mathbf{P}_i^- \cdot \mathbf{H}^T + \mathbf{R})^{-1}$; **Update gain**

$\mathbf{m}_i \leftarrow LoadObservation(i)$

$\hat{\mathbf{x}}_i = \hat{\mathbf{x}}_i^- + \mathbf{K}_i \cdot (\mathbf{m}_i - \mathbf{H} \cdot \hat{\mathbf{x}}_i^-)$; **Estimate the next state**

$\mathbf{P}_i = (\mathbf{I} - \mathbf{K}_i \cdot \mathbf{H}) \cdot \mathbf{P}_i^-$; **Update noise**

elihw

Algorithm 1: Kalman state estimator basic algorithm as presented in [12].

The key to use a KSE is the definition of the matrices $\mathbf{A}, \mathbf{B}, \mathbf{H}, \mathbf{Q}, \mathbf{R}$, the initialization vector $\hat{\mathbf{X}}_0$, the process noise vector $\mathbf{P}_0$, the time-depending input vector $\boldsymbol{u}_i$ and measurement vector $\mathbf{m}_i$. Furthermore, a stop criteria has to be defined in order to terminate the prediction-innovation loop. These definitions are discussed in the next section.

3.1.1 Kalman equations for vessel tracking and RGC construction

The matrices and vectors used in our KSE-based vessel tracking algorithm are:

- The measurement vector $\mathbf{m}$ contains the information needed to construct the vector defined in equation 3.

- The state vector $\mathbf{x}$ contains the information needed to construct the vector defined in equation 3, together with its velocity ($\mathbf{x}$ © [M M´]^{T}). In other words, it also describes RGC-sm pieces with the rate of change of each RGC-sm parameter.
- $\mathbf{u_i = 0}$ ^ $\mathbf{B = 0}$. In other words, there are no external inputs.
- A = $\begin{bmatrix} I & I \\ 0 & 0 \end{bmatrix}$: i.e. predicted pieces are just projections of previously estimated pieces, taking into account the velocity, as in the Newton's laws.
- $\mathbf{H = I}$: i.e. measured pieces, in the absence of noise, should be considered as good estimations.
- Experimentally, we fixed the noise covariance matrices to $\mathbf{Q} = 10^{-3}.\mathbf{I}$ and $\mathbf{R} = 10^{-3}.$ I.
- Accordingly, the initial process noise matrix $\mathbf{P_0} = 10^{-3}.\mathbf{I}$.

After each iteration, the estimated state $\hat{\mathbf{X}}_i$ is appended to the resulting RGC-sm, thus constructing the final cylindrical representation of the chosen vessel.

3.2 Retrieval of observations from image data

Without loss of generality, we explain the process for the first cylinder piece. Under the assumption of constant curvature and torsion, each piece of $\mathbf{H}$ is a helix, and a geometrical reasoning demonstrates that its parameters can be recovered if the frames Γ_0, Γ_1, at its extremities, as well as their origin locations $\mathbf{h_0}$ and $\mathbf{h_1}$, are available. Owing to a lack of space here, this reasoning will be given in a future publication. The remaining parameters are calculated using the Fourier decompositions of the contours Z_0 and Z_1. We first give main equations that lead from Γ_0 Γ_1 , $\mathbf{h_0}$, $\mathbf{h_1}$,Z_0 and Z_1 to the RGC-sm parameters. Then we explain the image processing steps that lead from the initial image and seed-points to these intermediate data.

3.2.1 Calculation of model parameters

We first compute the transition operators, respectively rotation and translation, between the extremities:

$$\mathbf{\Phi}(0,\Delta_0) = \mathbf{\Gamma}_0^{\mathrm{T}} \cdot \mathbf{\Gamma}_1, \qquad (7)$$

$$\mathbf{Tr}(0,\Delta_0) = \mathbf{\Gamma}_0^{\mathrm{T}} \cdot (\mathbf{h}_1 - \mathbf{h}_0). \qquad (8)$$

Φ is a rotation operator and one of the properties of the rotation matrices is the existence of Θ and Ξ such that $\Phi(0, \Delta_0) - \Phi(0, \Delta_0)^T = 2 \sin\Theta.\Xi$, where Θ is the rotation angle and the non-zero elements of the antisymmetric matrix Ξ compose the vector defining the rotation axis. Moreover, it can be demonstrated that $\Phi(t_1, t_2) = \exp((t_2 - t_1).\Psi)$, where Ψ is proportional to Ξ : $\Psi = \mu\Xi$. In the case where Φ describes the rotation between two frames attached to a helix, the coefficient μ is also involved in the calculation of the curvature and torsion of the helix. Indeed, these are proportional (via μ) to the cosine and sine of the angle φ that represents the "slope"' of the helix. Hence, the second step is the subtraction:

$$\mathbf{\Phi}(0,\Delta_0) - \mathbf{\Phi}(0,\Delta_0)^{\mathrm{T}} = \begin{bmatrix} 0 & -c & b \\ c & 0 & -a \\ -b & a & 0 \end{bmatrix}.$$

$$\Theta = \arcsin \frac{1}{2}\sqrt{a^2 + b^2 + c^2}$$

It can be demonstrated that *a, b, c* can be used to calculate φ, then μ:

$$\varphi = \arcsin\left(a/\sqrt{a^2 + b^2 + c^2}\right),$$

$$\mu = \frac{\sin\Theta\cos^2\varphi + \Theta\sin^2\varphi}{\left[\mathbf{\Phi}(0,\Delta_0)[1 \quad 0 \quad 0]^{\mathrm{T}}\right]^{\mathrm{T}}\mathbf{Tr}(0,\Delta_0)}$$

which in turn permits the computation of the axial parameters:

$$\begin{cases} \nu_0 = \arctan(b/c), \\ \kappa_0 = \mu\cos\varphi, \\ \tau_0 = \mu\sin\varphi, \\ \Delta_0 = \Theta/\mu. \end{cases} \quad (9)$$

Numerical stability problems might arise when $\Phi(0, \Delta_0) = \mathbf{I}$, which

occurs when $\mathbf{H}_0$ is a straight line segment. This is checked after the computation of Γ_0 and Γ_1, and the parameters, in this case, are set as follows: $[k_0\ \tau_0\ v_0\ \Delta_0]^T=[0\ 0\ 0\ |\boldsymbol{h}_1-\boldsymbol{h}_0|]^T$. The last step is the computation of the parameters describing the linear evolution of the Fourier decomposition of the contours:

$$\Lambda_0 = \left\{ \frac{Z_{1,l} - Z_{0,l}}{\Delta} \right\}_{C:-q \le l \le +q} . \quad (10)$$

3.3 Approximate axial shape extraction

As mentioned above, in the current implementation, the vessel tracking with Kalman estimation of RGC-sm parameters is performed along an initial approximate axis $\tilde{\mathbf{H}}$. The line $\tilde{\mathbf{H}}$, that coarsely describes the axial shape of the vessel, is constructed as follows:

1. A binary image[1] $\mathsf{B}(\mathbf{p})$, is computed from the initial image $f(\mathbf{p})$, using locally adaptive thresholds f_L , f_H that coarsely separate the vascular lumen from the background. These thresholds are defined using the results presented in [4]. According to that work, the vascular lumen intensities along the carotids have two properties: (a) the global lower threshold values are in the range [140HU, 420HU], and (b) the local threshold values vary almost linearly along the vessel axis. Using these properties, the lumen is segmented using a flooding algorithm that computes thresholds depending on the distance of each voxel to user-given seeds. The local threshold properties are computed using the Robust Automatic Threshold Selection (RATS) scheme [9].
2. An Euclidean distance map $\mathbf{E(p)}$, is computed within $\mathbf{B(p)}$ using the algorithm proposed in [10].
3. Finally, a cost function $\mathbf{F}(\mathrm{p}) = \frac{1}{1+\mathbf{E(p)}}$ is used for a minimal path algorithm (as proposed in [13]), which finds a set $\tilde{\mathbf{H}}$ of points ordered along the shape and connecting the seed-points even in the presence of lumen discontinuities (severe stenoses). These points are expected to be located near the center of the vessel due to the cost function $\mathbf{F(p)}$, related to the distance map $\mathbf{E}(\mathbf{p})$

3.4 Contours extraction

The planar contours are extracted using the fast marching (FM) method [11]. FM is a front propagation technique that provides a set of (counter-clockwise) ordered points $\mathsf{C}_i = \{c_{i,k} : 0 \le k < K\}$. This technique needs

1 From hereafter we suppose that images are functions defined in a n-dimensional space: $f(\boldsymbol{p})$: $\mathsf{R}'' \Rightarrow \mathsf{R}$, where $\boldsymbol{p}$ are the pixels of the image.

the definition of a potential field $P(\mathbf{p})$ expected to be maximum at discontinuities (edges) and minimum within uniform regions. We use the potentials proposed in [2], where the native image intensities $f(\mathbf{p})$ along with image discontinuities represented by the gradient magnitude $f(\mathbf{p})$ are used:

$$P(\mathbf{p}) = \frac{|f(\mathbf{p})|}{K(d(\mathbf{p}), \alpha_1, \beta_1)\, K(f(\mathbf{p}), \alpha_2, \beta_2)\, K(f(\mathbf{p}), \alpha_3, \beta_3)} \quad (11)$$

The function $K(.)$ of a scalar μ is defined as follows:

$$K(u, \alpha, \beta) = 1 + \exp\left(-\frac{u-\alpha}{\beta}\right), \quad (12)$$

where α is a shift, β is a signed sharpness parameter and $d(\mathbf{p})$ is a mono-dimensional derivative of $|f(\mathbf{p})|$ along the direction normal to the front. With $\alpha_1 = 0$, $\alpha_2 = f_l$, $\alpha_3 = f_H$, $\beta_1 = 100$, $\beta_2 = 1$ and $\beta_3 = -1$, this potential function P strongly decreases the propagation speed when the front moves beyond local maxima of the gradient norm (i.e. beyond borders of the arteries) or beyond the range $[f_l, f_l]$ of luminal intensities, defined as described in previous subsection. Furthermore, in this work the authors recommend that the FM propagation should be stopped at time value T when the growth of the area A encompassed by the front becomes very slow, which is characterized by a large value of $\Delta T/\Delta A$. Actually, at each iteration we compute the mean $m_{T/A}$ and the standard deviation $\sigma_{T/A}$ of $\Delta T/\Delta A$ and the propagation stops when $\Delta T/\Delta A > m_{T/A} + 10\,\sigma_{T/A}$. All the coefficient settings correspond to the experimental values from [2].

Front propagation is performed in the plane passing through the predicted point $\hat{h}_i \in \tilde{H}$, and oriented according to the predicted vessel orientation expressed by the orthogonal base $\hat{\Gamma}_i$. Summarizing, the point set C_i is extracted as follows:

1. The potential field $\mathbf{P}(\mathbf{p})$ is sliced by the plane passing by $\hat{\mathbf{h}}_i$ and oriented by the first column vector of $\hat{\Gamma}_i$, to obtain a 2D image $\mathbf{Q}_i(\mathbf{p})$.
2. The FM algorithm is executed on $\mathbf{Q}_i(\mathbf{p})$ with $\hat{\mathbf{h}}_i$ as the first trial point (front initialization).

3. The FM generates the level set $\mathbf{L}_i(\mathbf{p})$ which contains $\mathbf{C}_i$ as its last level.

The initialization of the RGC-sm reconstruction process requires $\mathbf{h}_0$, Γ_0 and $\mathbf{Z}_0$. One of the seed-points (typically the distal one) is taken as $\mathbf{h}_0$. The orthonormal basis Γ_0 is constructed such that its first vector is tangent to $\tilde{\mathbf{H}}$ in $\mathbf{h}_0$, the second vector is oriented along $\mathbf{h}_0 - \mathbf{C}_{0,0}$, and the third one is orthogonal to both. $\mathbf{Z}_0$ is calculated as the Fourier series corresponding to $\mathbf{C}_0$, using the harmonics up to the third order ($q = 3$), which is sufficient to represent reasonably complex cross-sections.

Stenosis quantification from the reconstructed model involves an analytic calculation of the cross-sectional areas directly from Fourier coefficients, while the diameters are computed from discrete contours.

4 Results

Both lumen segmentation and stenosis quantification were evaluated on 15 training and 31 testing carotid CTA datasets available within the Carotid Bifurcation Algorithm Evaluation Framework. Details of the evaluation methodology can be found on the web page of the challenge [5]. Figure 5 displays an example of segmentation result.

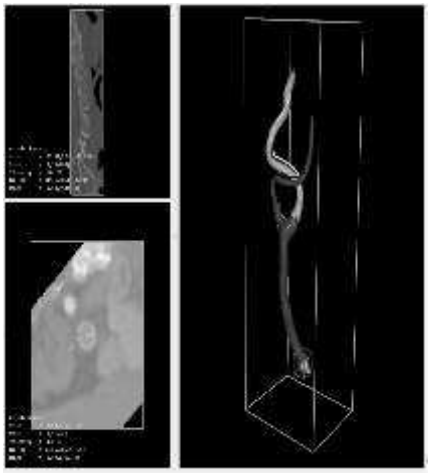

Figure 5: Example of the segmentation of a CTA image of a carotid using our algorithm. The internal carotid is presented in cyan and the external carotid is presented in red. The yellow and blue lines represent the generating curves calculated.

Stenosis quantification was evaluated by calculating the difference between the calculated percentage and the one provided by the reference standard, using both cross-sectional areas and diameters. The results are presented in table 1.

Four criteria were evaluated to assess the lumen segmentation: Dice similarity index, mean surface distance, RMS surface distance and maximal surface distance. Table 2 summarizes the results obtained.

The average running time of our algorithm, including lumen segmentation, stenosis grading and display of intermediate and final results, was 3.7 ∠1.3 minutos.

Team name	area %	diam %
Our method	32.76	40.31
ObserverA	2.71	3.61
ObserverB	4.55	5.29
ObserverC	5.61	5.74

Table 1: Testing stenosis.

Team name	dice %	msd mm	rmssd mm	max mm
Our method	51.8	3.42	4.29	9.46
ObserverA	95.4	0.10	0.13	0.56
ObserverB	94.8	0.11	0.15	0.59
ObserverC	94.7	0.11	0.15	0.71

Table 2: Averages testing lumen.

5 Discussion and conclusion

RGC-sm is a powerful tool that permits a concise description of complex generalized cylindrical shapes. The theoretical framework permits the reconstruction of a continuous surface corresponding to the lumen, based on a limited number of discrete contours. Additionally, the Kalman estimator permits a correction of the observation errors when these remain within a reasonable range. However, our current implementation of the image processing steps devised to provide the observations is clearly not optimal. The initial rough extraction of the axial shape begins by a thresholding step, which is prone to errors when neighboring structures have a similar intensity range. Actually, this initial curve needs to be quite well-centered within the lumen. Indeed, as the Fast Marching algorithm in planes orthogonal to this initial curve

starts from the intersection between the plane and the curve, this intersection has to fall within the lumen, otherwise the contour extraction fails. Failures are also observed when the curve is located within the lumen, close to a poorly contrasted boundary. In fact, the use of an always inflating deformable contour, such as the Fast Marching front, is uneasy, since the speed function and stopping criteria hardly can cope with all possible configurations (nearby veins, calcifications, etc.). Furthermore, 2D Fast Marching does not exploit the 3D continuity of the vascular lumen, which might be helpful in some complicated situations. Future work will be oriented towards an implementation that do not require the initial extraction of an approximate axial shape and that perform a piece-wise local 3D boundary extraction. Let us also note that the current implementation was designed with an implicit assumption (constraint) that the seed-points are also end-points, and are given at "easy" locations, *i.e.* healthy circular cross-sections without neighboring structures "stuck" to the artery of interest. Hence, the method had difficulties in datasets where the seed-point in the internal carotid artery was located either close to the bifurcation, so that our method segmented a too short part of the artery, or near the skull where the assumption of the absence of neighboring structures did not hold. Further work is necessary to cope with seed-points located anywhere within the vessel of interest.

References

[1] Azencot, J. and Orkisz, M. Deterministic and stochastic state model of right generalized cylinder (RGC-sm): application in computer phantoms synthesis. *Graph. Models*, 65(6):323--350, 2003.

[2] Baltaxe Milwer, M. and Flórez Valencia, L. and Hernández Hoyos, M. and Magnin, I.E. and Orkisz, M. Fast marching contours for the segmentation of vessel lumen in CTA cross-sections. *Conf. Proc. IEEE Eng. Med. Biol. Soc.*, pages 791-794, Lyon, France, 2007. IEEE.

[3] Flórez Valencia, L. and Azencot, J. and Vincent, F. and Orkisz, M. and Magnin, I.E. Segmentation and Quantification of Blood Vessels in 3D Images using a Right Generalized Cylinder State Model. *Proc. IEEE Int. Conf. Image Process.*, pages 2441--2444, 2006.

[4] Flórez Valencia, L. and Vincent, F. and Orkisz, M. Fast 3D pre-segmentation of arteries in computed tomography angiograms. *Int. Conf. Comput. Vision & Graphics*, pages 87--88, Warsaw, Poland, 2004.

[5] Hameeteman, K. and Zuluaga, M. and Joskowicz, L. and Freiman, M. and van Walsum, T. 3D Segmentation in the Clinic: Carotid Lumen Segmentation and Stenosis Grading Challenge. 2009. http://cls2009.bigr.nl.

[6] Hernández Hoyos, M. and Orkisz, M. and Douek, P.C. and Magnin, I.E. Assessment of carotid artery stenoses in 3D contrast-enhanced magnetic resonance angiography, based on improved generation of the centerline. *Mach. Graphics Vision*, 14(4):349--378, 2005.

[7] Kakadiaris, I.A. and Pednekar, A. and Santamaría-Pang, A. Three-dimensional shape-motion analysis of the left anterior descending coronary artery in EBCT images. In Barillot, C. and Haynor, D.R. and Hellier, P., editors, *MICCAI*, pages 1025--1033, 2004. Springer.

[8] Kalman, R.E. A New Approach to Linear Filtering and Prediction Problems. *Trans ASME--J. Basic Engineering*, 82(Series D):35--45, 1960.

[9] Josef Kittler and John Illingworth and J. Föglein. Threshold selection based on a simple image statistic. *Comput. Vision Graphics Image Process.*, 30(2):125-147, 1985.

[10]Maurer,Jr., Calvin R. and Qi, Rensheng and Raghavan, Vijay. A Linear Time Algorithm for Computing Exact Euclidean Distance Transforms of Binary Images in Arbitrary Dimensions. *IEEE Trans. Pattern Anal. Mach. Intell.*, 25(2):265--270, 2003.

[11]Sethian, J.A. A Fast Marching Level Set Method for Monotonically Advancing Fronts. *Proc. Nat. Acad. Sci.*, number 4, pages 1591--1595, 1996.

[12]Welch, G. and Bishop, G. An Introduction to the Kalman Filter. SIGGRAPH 2001, Course 8, Chapel Hill, NC, 2001.

[13]Wink, O. and Niessen, W.J. and Frangi, A.F. and Verdonck, B. and Viergever, M.A. 3D MRA coronary axis determination using a minimum cost path approach. *Magnetic Resonance in Medicine*, 47(6):1169--1175, 2002.